Asociación Argentina
de Mecánica Computacional

Mecánica Computacional Vol XXVII, págs. 265-280 (artículo completo)
Alberto Cardona, Mario Storti, Carlos Zuppa. (Eds.)
San Luis, Argentina, 10-13 Noviembre 2008

MACROSCOPIC MODELING OF TURBULENCE IN POROUS MEDIA FLOWS

Federico E. Teruel[a], Rizwan-Uddin[b]

[a]*Centro Atómico Bariloche, CNEA, Bariloche 8400, Rio Negro, Argentina, teruel@cab.cnea.gov.ar, http://www.cab.cnea.gov.ar*
[b]*Department of Nuclear, Plasma and Radiological Engineering, University of Illinois at Urbana-Champaign, Urbana, IL 61801, USA, rizwan@uiuc.edu.ar, http://www.ne.uiuc.edu*

Keywords: Turbulence modeling, Porous media, *k-epsilon* model, Volume averaging.

Abstract. A new model to describe turbulent flows within the porous media approximation is presented. The spatial- and time fluctuations in this new model are tied together and treated as a single quantity. This novel treatment of the fluctuations leads to a natural construction of the "*k*" and "*epsilon*" type equations for rigid and isotropic porous media in which all the kinetic energy filtered in the averaging process is modeled. The same terms as those found in the corresponding equations for clear flow, plus additional terms resulting from the interaction between solid walls in the porous media and the fluid characterize the model. These extra terms arise in a boundary integral form, facilitating their modeling. The model is closed by assuming the eddy viscosity approximation to be valid, and using simple models to represent the interaction between the walls in the porous media and the fluid. Preliminary validation of the model is carried out by simulating a free stream entering to an infinite two dimensional porous medium formed by staggered squares (numerical solution based on Reynolds Averaged Navier-Stokes equations, RANS). Simulations are carried out for the 75% porosity case. Different inlet turbulence intensities are imposed on the free stream to test the model under different macroscopic boundary conditions. Microscopic RANS solutions for the turbulence quantities (*k* and *epsilon*) are averaged in space and compared with those yielded by the porous media model. The model is shown to fairly predict macroscopic turbulence quantities under different testing conditions. Results encourage further validation of the model in more complex porous media geometries.

1 INTRODUCTION

The analysis of fluid flowing through porous media is required in a large range of applications in such industries as chemical, mechanical, nuclear, geological, environmental, petroleum, etc. The pore-size's spectrum is vast and can vary from the order of Å (ultra-micro-pores) to cm (pebbles, food) or even larger (Kaviany, 1991). Moreover, the conditions encountered in different applications are broad enough to cover a large range of Reynolds numbers. For example, Stokes type flows in porous media may be encountered in ground water flows while turbulent flows are found in application such as heat exchangers or nuclear reactors. Due to lack of geometric information to model each and every pore, such systems are difficult to simulate with full geometric details. Despite the fact that it might be possible to describe some of these systems in an almost exact representation or a meaningful statistical approximation of the geometry, the computational effort required to solve the flow field in such geometries is still out of reach. This motivates the research in the development of porous media approximation, representing the system composed of pores by a macroscopic homogenous one with uniform properties. While both, laminar and turbulent, flows are important (Lopez and Garcia, 2001; Becker and Laurien, 2003; Nakayama et al. 2004; Chandesris et al., 2006), number of modeling efforts reported for turbulent flows in porous media is relatively small.

Most approaches to model turbulent flow in porous media are based on the approaches usually followed to model turbulence in clear flows (Masuoka and Takatzu, 1996; Antohe and Lage, 1997; Nakayama and Kuwahara, 1999; Pedras and de Lemos, 2001). Not surprisingly, the most common approach is to extend the k-ε model. Since a region of space occupied by solid and fluid, in the porous media approximation is represented by a "homogenized" region, results obtained using such models are relevant only at the macroscopic scale. Space-fluctuating quantities in addition to the Reynolds decomposition are then introduced in the macroscopic representation (Rapauch and Shaw, 1982).

Turbulence (k-ε type) models for porous media developed earlier differ from each other because they are based on different definitions of the macroscopic turbulence quantities, such as the turbulent kinetic energy and the dissipation rate (Pedras and de Lemos, 2000). For example, the introduction of different macroscopic or space averaged quantities lead to different spatial correlations (in addition to the well known time fluctuations found in turbulent flows in clear media). Unfortunately, relevant microscopic experimental data is scarce, and hence any comparative analysis of these models and space-averaged quantities must be based on an evaluation of the assumptions employed in the development, simplicity of the model, and, when available on comparison of macroscopic results predicted by the models with experimental data. For example, one limitation of these models is that only a part of the kinetic energy filtered in the averaging process is captured by the transport equation. Hence, a model that is free of this limitation is desirable.

The approach followed here in developing a new model for turbulent flow in porous media (Teruel and Rizwan-uddin, 2006; Teruel, 2007) is based on redefining the turbulence quantities, and consequently their transport equations in the k-ε turbulence model, in such a way that time and space fluctuations are not specifically distinguished. These new definitions of the turbulence quantities lead to a model in which all of the kinetic energy filtered in the space-time averaging process is modeled in its transport equation. Moreover, the resulting model is simple: the definition leads to a natural construction of the k and ε equations, with the same terms found in the corresponding equations for clear flow, plus additional (boundary) terms resulting from the interaction between solid walls of the porous media and the fluid.

Organization of the paper is as follows. An introduction to the space or volume averaging approach generally used in modeling porous media is given. A new set of equations developed by treating the average over space- and time fluctuations as a unique quantity is presented (Teruel and Rizwan-uddin, 2006). The study is then devoted to the determination of model constants and validation of these equations. A numerical experiment similar to the one carried out by Nakayama and Kuwahara (1999) is carried out to validate the spatial evolution of macroscopic turbulence quantities predicted by the model. The RANS equations (microscopic simulation) are solved for the case of a unidirectional flow entering the porous medium considered in this study. The spatial evolution of the relevant macroscopic quantities can then be obtained by appropriate averaging of the microscopic results. Macroscopic porous media turbulence equations are also solved for the same problem. Results obtained using the latter approach are compared with those obtained using the microscopic simulations.

2 MACROSCOPIC VARIABLES AND SPACE-TIME AVERAGED QUANTITIES

The notion of space average in porous media is based on the assumption that although fluid velocities and pressure may be irregular at the pore scale, locally space-averaged measurements of these quantities vary smoothly (Whitaker, 1999). Macroscopic equations are commonly obtained by spatially averaging the microscopic ones over a Representative Elementary Volume (REV) of the porous media. A REV should be the smallest differential volume that results in meaningful local average properties (Kaviany, 1999). This implies that the length scale of this volume should be considerably larger than the pore scale. In addition, the dimension of the system should be considerably larger than the REV's length scale to avoid gross inhomogeneities. Mathematically, this can be expressed as:

$$p << D << L\,, \tag{1}$$

where p is the pore scale or microscopic length scale, D is the macroscopic length scale and L is the megascale or scale of the system (see Figure 1).

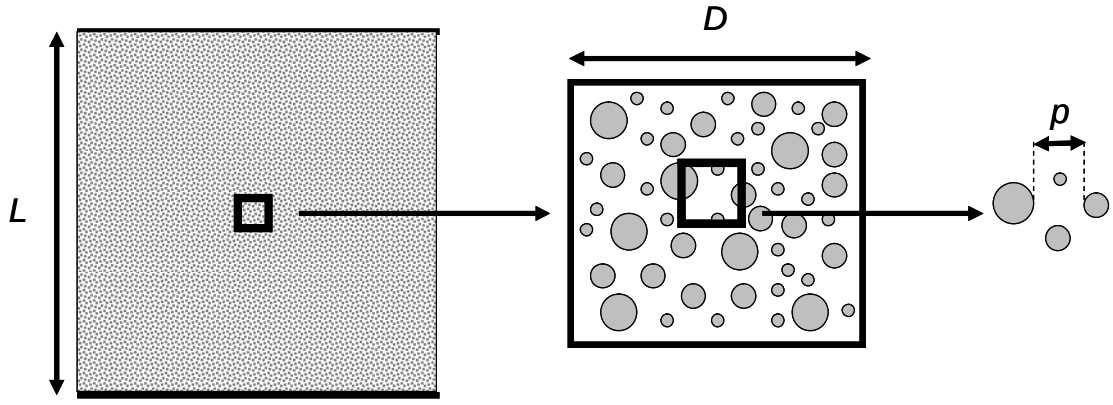

Figure 1. Identification of different length scales.

In a particular system, precise a priori identification of each length scale may be difficult, but one criterion that must be fulfilled is that macroscopic quantities determined using the model must be insensitive to small changes in the size of the volume over which local averaging is carried out (Kaviany, 1999).

A schematic representation of a spherical REV consisting of a fixed solid phase saturated with a continuous fluid phase is shown in Figure 2 (note that the solid phase is fixed, that is,

the solid phase does not change randomly if different ensembles are considered). The volume of the REV is constant (no space dependence) and its value is equal to the sum of the fluid and solid volumes inside the REV ($V = V_f + V_s$). For averaging purposes, an auxiliary coordinate system $r = x + \xi$ is defined, so that x describes the origin of each averaging volume and ξ is the position in a local coordinate system specific to each averaging volume. In this treatment, the ideas of Hassanizadeh and Gray (1979) and Gray et al. (1993) are followed.

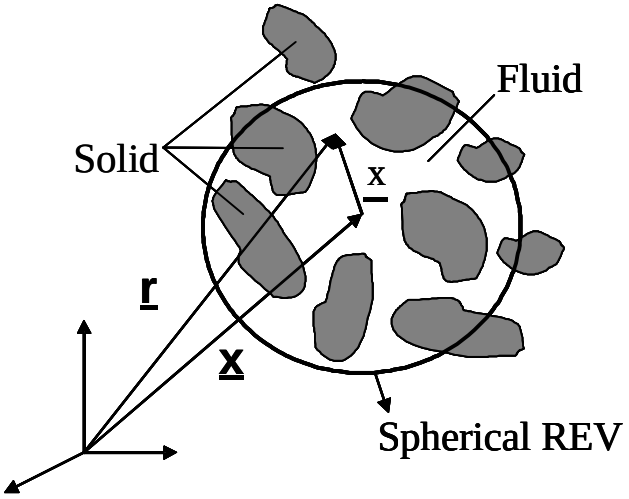

Figure 2. Spherical representative elementary volume (REV).

Defining a distribution function $\gamma_f(r)$, as one in the fluid phase and zero in the solid phase,

$$g_f(\underline{r}) = \begin{cases} 1 & if\ \underline{r} \in V_f \\ 0 & if\ \underline{r} \in V_s \end{cases}, \tag{2}$$

the cell-average $\langle\psi\rangle$, and the intrinsic phase cell-average $\langle\psi\rangle^f$ of any quantity $\psi(r,t)$ associated with the fluid (scalar, vector or second order tensor) can be defined as:

$$\langle y \rangle(\underline{x},t) = \frac{1}{V}\int_V y\,(\underline{x}+\underline{z},t)\, g_f(\underline{x}+\underline{z})\, dV_z \quad , \tag{3}$$

$$\langle y \rangle^f(\underline{x},t) = \frac{V}{V_f(\underline{x})}\langle y \rangle(\underline{x},t) = \frac{\langle y \rangle(\underline{x},t)}{f(x)}, \tag{4}$$

where the porosity $f(x)$, is defined as:

$$f(\underline{x}) = \frac{1}{V}\int_V g_f(\underline{x}+\underline{z})\, dV_z = \frac{V_f(\underline{x})}{V} \quad . \tag{5}$$

It may be useful for the reader familiar with the averaging performed in Large Eddy Simulations (LES) to consider the cell-average quantity, $\langle\psi\rangle$, as a filtered quantity, where $\gamma_f(r)$ is the filter function. However, for the porous media case, it is important to note that although the quantity ψ may only be defined in the fluid space, its space average is defined everywhere (the integration performed in equation (3) is meaningful considering that $\psi \times \gamma_f = 0$ in the solid phase).

As originally defined in Hassanizadeh and Gray (1979), a quantity $\psi(r,t)$ associated with the fluid may be decomposed in an intrinsic phase cell-average value $\langle y \rangle^f(x,t)$ plus a local

fluctuation in space ${}^{i}y(x,t)$:

$$y\,(\underline{r},t) = \langle y \rangle^{f}(\underline{x},t) + {}^{i}y\,(\underline{r},\underline{x},t)\,. \tag{6}$$

Under the length scale constraint of equation (1) it is shown that the intrinsic phase cell-average quantity is approximately constant inside the REV (Whitaker, 1969; Whitaker, 1999):

$$\left\langle {}^{i}y \right\rangle \cong 0 \quad , \quad \left\langle \langle y \rangle^{f} \right\rangle^{f} \cong \langle y \rangle^{f}\,. \tag{7}$$

And therefore, decomposition in equation (6) represents a separation of length scales where space averaged quantities are approximately constant inside the REV.

To describe turbulence within porous media flows, not only the space averaging operator is employed but also time averaging. Therefore, any fluid quantity is space-time averaged to yield a macroscopic variable as:

$$\overline{\langle y \rangle^{f}}(x,t) = \frac{1}{\Delta t}\int_{\Delta t}\left[\frac{1}{V_f}\int_{V_f} y\ dV\right]dt = \frac{1}{V_f}\int_{V_f}\left[\frac{1}{\Delta t}\int_{\Delta t} y\ dt\right]dV = \overline{\langle y \rangle}^{f}(x,t)\,. \tag{8}$$

Therefore, the space-time averaged quantity captures time fluctuations of space averaged quantities inside the REV and space fluctuations of quantities of time averaged quantities inside the cell.

3 MACROSCOPIC TURBULENCE MODEL

The characteristic features of the new model are summarized in this section. For details, refer to Teruel (2007). The fluctuations in this model are defined with respect to space-time averaged quantities (see equation 8). For any flow variable y, the following decomposition is introduced:

$$y\,(\underline{r},t) = \overline{\overline{y}}\,(\underline{x},t) + y''(\underline{r},\underline{x},t)\,, \tag{9}$$

where

$$\overline{\overline{y}}\,(\underline{x},t) = \frac{1}{\Delta t}\int_{\Delta t}\left[\frac{1}{V_f}\int_{V_f} y\ dV\right]dt = \frac{1}{V_f}\int_{V_f}\left[\frac{1}{\Delta t}\int_{\Delta t} y\ dt\right]dV\,, \tag{10}$$

[note that double bars have been introduced to indicate space-time averaging, equation 8.]
With this definition of the fluctuation, the Macroscopic Turbulent Kinetic Energy (MTKE, k) is defined as:

$$k = \frac{\overline{\overline{u_j'' u_j''}}}{2} = \frac{\left\langle \overline{u_j' u_j'} \right\rangle^{f}}{2} + \frac{\left\langle {}^{i}\overline{u}_j\, {}^{i}\overline{u}_j \right\rangle^{f}}{2} = k_{NK} + k_{DISP}\,, \tag{11}$$

showing that k is equal to the space average of the microscopic Turbulent Kinetic Energy (TKE, k_{NK}) plus the dispersive kinetic energy (k_{DISP}) or space dispersion of the mean (time average) flow. Similarly, the Macroscopic turbulent Dissipation Rate (MDR) is naturally defined in the new model as:

$$e = n\overline{\overline{\frac{\partial u_i''}{\partial x_j}\frac{\partial u_i''}{\partial x_j}}} = n\left\langle\overline{\frac{\partial u_j'}{\partial x_j}\frac{\partial u_j'}{\partial x_j}}\right\rangle^f + n\left\langle\frac{\partial^i\overline{u}_i}{\partial x_j}\frac{\partial^i\overline{u}_i}{\partial x_j}\right\rangle^f = e_{NK} + n\left\langle\frac{\partial^i\overline{u}_i}{\partial x_j}\frac{\partial^i\overline{u}_i}{\partial x_j}\right\rangle^f, \quad (12)$$

where ε_{NK} is the space average of the microscopic Turbulent Dissipation Rate (TDR).

The complete set of equations for the case of isotropic and constant porosity porous medium, the one-equation and two-equation models, is given by:

$$\frac{\partial\overline{\overline{u}}_i}{\partial x_i} = 0, \quad (13)$$

$$\frac{D\overline{\overline{u}}_i}{Dt} = -\frac{1}{r}\frac{\partial(\overline{\overline{p}} + 2/3k)}{\partial x_i} + \frac{\partial}{\partial x_j}[(n + n_T)\frac{\partial\overline{\overline{u}}_i}{\partial x_j}] + R_i, \quad (14)$$

$$\frac{Dk}{Dt} = -\overline{\overline{u_j''u_i''}}\frac{\partial\overline{\overline{u}}_i}{\partial x_j} + \frac{\partial}{\partial x_j}[(n + \frac{n_T}{s_k})\frac{\partial k}{\partial x_j}] - e - \overline{\overline{u}}_i R_i, \quad (15)$$

with:

$$R_i = -\frac{fn}{K}\overline{\overline{u}}_i - \frac{f^2F}{\sqrt{K}}\sqrt{\overline{\overline{u_ju_j}}}\,\overline{\overline{u}}_i \quad ; \quad \overline{\overline{u_i''u_j''}} = -n_T(\frac{\partial\overline{\overline{u}}_i}{\partial x_j} + \frac{\partial\overline{\overline{u}}_j}{\partial x_i}) + \frac{2k}{3}d_{ij}. \quad (16)$$

For the one-equation model:

$$e = C_D\frac{k^{3/2}}{l_m} \quad and \quad n_T = c\,k^{1/2}l_m, \quad (17)$$

and for the two-equation model:

$$\frac{De}{Dt} = -C_{e1}\frac{e}{k}\overline{\overline{u_j''u_i''}}\frac{\partial\overline{\overline{u}}_i}{\partial x_j} + \frac{\partial}{\partial x_j}[(\frac{n_T}{s_e} + n)\frac{\partial e}{\partial x_j}] - C_{e2}\frac{e^2}{k} + f(f,K)\frac{e\sqrt{\overline{\overline{u_ju_j}}}}{\sqrt{K}}, \quad (18)$$

$$n_T = C_m\frac{k^2}{e}. \quad (19)$$

4 MODEL CHARACTERISTICS UNDER DEVELOPING CONDITIONS

4.1 Determination of model constants and model validation

In this study, a numerical experiment similar to the one carried out by Nakayama and Kuwahara (1999) is carried out to determine the model parameters and to validate the model. The RANS equations (microscopic simulation) are solved for the case of the unidirectional flow entering the porous medium shown in Figure 3. The spatial evolution of the relevant macroscopic quantities is then obtained by space averaging the microscopic results. Macroscopic equations are also solved for the same problem and the macroscopic results are then compared with the corresponding variables obtained using the microscopic simulations.

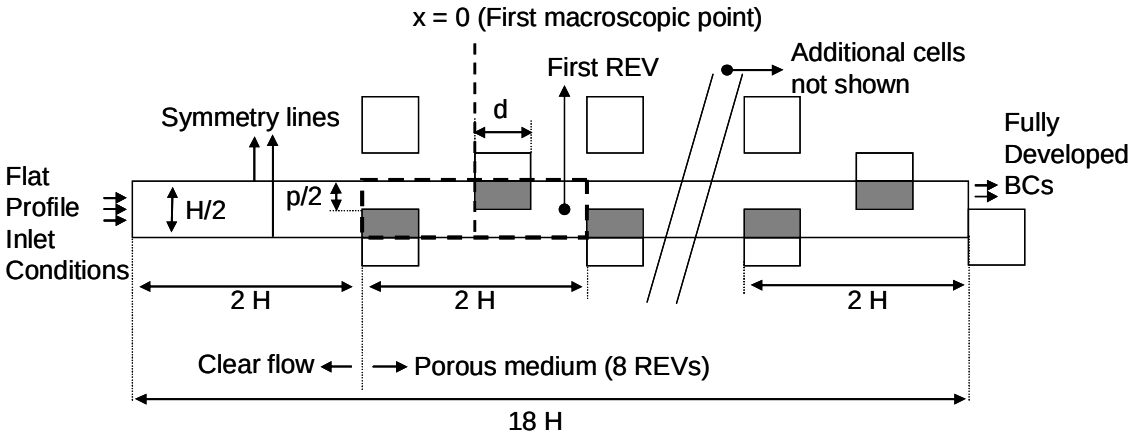

Figure 3. Geometry of the domain simulated for the case of a free stream entering the porous medium (*18H x H/2*).

The fact that the macroscopic turbulence quantities, such as the MTKE and MDR, are significantly different from those defined for clear flows (i.e. macroscopic quantities are quantities averaged in space) suggests that model parameters introduced in the macroscopic model (C_{e1}, C_{e2}, C_m, s_k, s_e ; see equations 13-19) may differ significantly from corresponding parameters usually found in models for clear flows. Moreover, model parameters may also depend on the geometry of the porous medium. Therefore, in this study, model parameters are determined by minimizing the difference between the macroscopic and space-time averaged microscopic results. Details are given in Sections 4.5, 4.6 and 4.7. Moreover, as model parameters should be independent of the boundary conditions, the minimization process is carried out over a space of different sets of boundary conditions.

4.2 Microscopic simulations of turbulent flow in the porous medium

Schematic diagram of the domain selected for simulation and comparison is shown in Figure 3. The fluid flows from left to right, entering the porous medium after flowing a distance of *2H* as clear flow. The porous medium extends for a distance of *16H* (i.e. eight REVs in a row), making the length of the domain in the streamwise direction equal to *18H*. To save computational time, and based on the fact that simulations of the REV at high *Re* numbers with periodic boundary conditions result in symmetric results (steady solutions, Teruel, 2007; Nakayama and Kuwahara, 1999), only the bottom half of the REV (*H/2*) is simulated, with symmetry boundary conditions (BCs) applied over the horizontal boundaries of the system.

The Semi-Implicit Method for Pressure Linked Equations Revisited (SIMPLER) algorithm developed by Patankar (1980) is used to solve the RANS equations. Central differences and the Quadratic Upstream Interpolation for Convective Kinematics (QUICK) scheme (Leonard, 1979; Hayase et al. 1982) are employed to respectively model the diffusion and the convective terms. Crank-Nicholson or the backward Euler scheme is used to advance in time. The k-ε model with near wall treatment developed by Abe et al. (1994) is used to model the Reynolds stresses. The solver has been fully tested and validated for geometries including those presented in this study as well as for a large range of Reynolds numbers. Additional details are available in (Teruel, 2007).

Domain is discretized using a non-uniform but structured grid of rectangles. A systematic grid refinement study was carried out. Results reported here are only those that were found to be independent of any further grid refinement (Teruel, 2007). The grid resolution employed for

each REV, shown in Figure 3, was 192 x 48 (streamwise x vertical direction). In addition to the grid refinement study, simulations were also carried out to study the impact of the height of the first cell. Uniform profiles of the relevant quantities in the entire domain are used as initial conditions. Variables are evolved over time up to the steady state. [All simulations evolved to steady state solutions.]

The *Re* number is set at 10^4 (based on the mass flow rate) and only the case of 75% porosity is presented here. A total of six simulations, corresponding to six different Boundary Conditions (BCs) or sets of BCs were carried out. Although the inlet velocity profile is the same for each simulation, the turbulence intensity at the inlet was varied to obtain different flow distributions in the porous medium and, consequently, different macroscopic solutions. Table 1 shows selected inlet boundary values for each turbulence quantity simulated, as well as the corresponding turbulence intensity and the ratio of the eddy viscosity to the fluid viscosity that resulted for each set.

BC	k	ε	I (%)	ν_T / ν
Set 1	1.00E-05	3.16E-08	0.26	2.8
Set 2	1.00E-04	1.00E-06	0.8	9.0
Set 3	1.00E-03	3.16E-05	2.6	28.5
Set 4	1.00E-02	1.00E-03	8.2	90.0
Set 5	1.00E-01	3.16E-02	25.8	284.6
Set 6	5.00E-01	3.54E-01	57.7	636.4

Table 1. Microscopic turbulence quantities for six sets of inlet boundary conditions.

It is important to note that the macroscopic boundary conditions in this study are calculated based on the solutions of the RANS equations. The macroscopic boundary conditions are evaluated by space averaging the microscopic solution in the first REV defined inside the porous medium (see Figure 3). Note that although any macroscopic boundary condition may be imposed on the macroscopic model, this does not assure that the imposed values are actually realizable in an experiment (i.e. they result from the space-time averaging of a solution of the Navier-Stokes, N-S, equations).

4.3 Microscopic results and expectations for macroscopic behavior

Though the purpose of the microscopic simulation is to compare the macroscopic results obtained by space averaging the microscopic results with the macroscopic results obtained using the macroscopic turbulence model, nevertheless, it is important to outline the salient features of the microscopic spatial evolution of the flow in the porous medium to facilitate the understanding of the space averaged values presented later. Figure 4 shows the distribution of the TKE (a), the distribution of the TDR (b) and the streamlines of the mean flow in (c), for Set 1 of BCs given in Table 1. The spatial evolution of the TKE—which for this set of BCs is low at the entrance (blue color) relative to the fully developed level (red color)—is determined by the flow interaction with the walls, and reaches its equilibrium distribution inside the REV. The volume average of the TKE is hence expected to evolve from a low value at the inlet to a larger fully developed one. Thus, the MTKE, as defined in this study, is not only dependant on the volume average of the TKE but also on the hydrodynamic dispersion of the mean flow. Interpretation of this quantity is facilitated by considering the REVs shown in Figure 4 (c). The first REV that the fluid passes through (top) shows a more complex distribution of eddies than

the REV downstream where the conditions are fully developed (bottom). Therefore, the hydrodynamic dispersion is larger in the entrance region, and it is expected to decay to a constant lower value downstream. The close relationship between the TKE and the distribution of the mean flow inside the REV is expected to be captured by the definition of the MTKE employed by the present model.

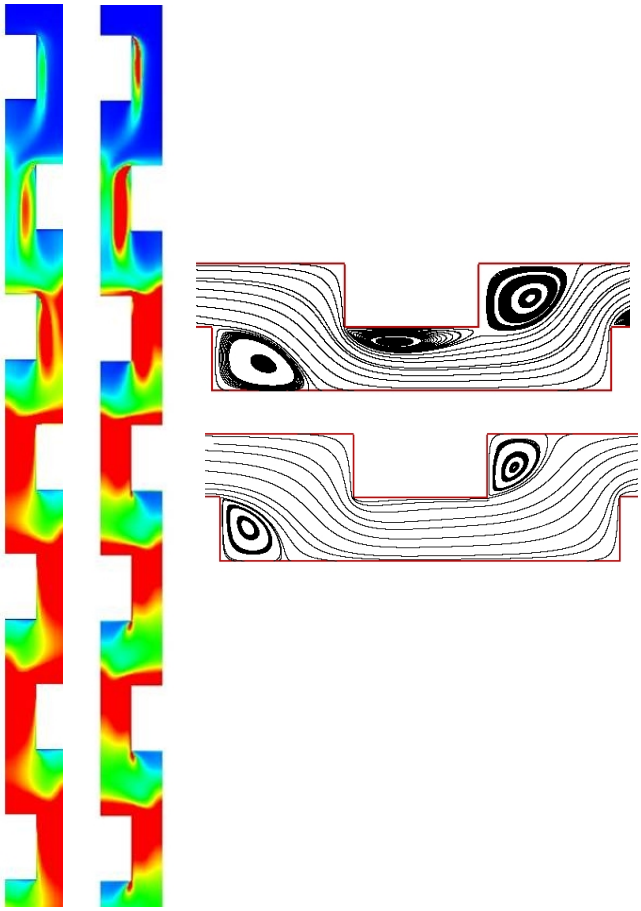

(a) (b) (c)

Figure 4. Distribution of the microscopic TKE (a), and TDR (b) (the fluid is flowing from top to bottom). Blue and red colors correspond to nondimensional levels of 0.0 and 0.25, respectively. Streamlines for two REVs are shown in (c). The top panel corresponds to the first REV in the domain, and the bottom one shows the fully developed condition. These results are for BC Set 1.

Insight in the macroscopic dissipation rate can be also be gained by analyzing the spatial evolution of the microscopic turbulence dissipation rate. Here it is worth recalling the fact that the dissipation of the mean flow is relatively small compared to the turbulence dissipation rate at this *Re* number. The turbulence dissipation rate evolves in a fashion similar to that of the TKE. The macroscopic TKE appears to increase monotonically to its equilibrium value.

4.4 Conversion of quantities from microscopic to macroscopic

As pointed out by Gray et al. (1993), a precise identification of different scales in a particular system is very difficult, and no precise criterion exists for this purpose. As a general criterion, the scale of the REV should be such that the averaged quantity is fairly insensitive to small changes in the size of the averaging volume. Additionally, it should not be dominated by the fluctuations at the pore scale nor smoothed over the global scale of the system. The flow

characteristics in the streamwise direction shown in Figure 4 suggest that the large scale of the system is approximately *10H* (i.e. no variation is found beyond this scale). The small scale of the system is approximately given by the size of the square edge (*d*, see Figure 3) or the vertical distance between the squares (*p*, see Figure 3). These length scales are unfortunately not much smaller than *H*. Therefore, in this problem, the scale separation is not naturally well defined. However, as the volume averaged quantities behave rather well for an intermediate scale (~ *2H*) (Teruel, 2007), the comparison between the macroscopic model and the spatial average of the microscopic results is carried out over this scale. In addition, it should be noted that the cell averaging has been shown to be sufficient for periodic structures (Quintard and Whitaker, 1994).

The spatial evolution of the macroscopic turbulence quantities is then computed by averaging the microscopic solution over the REV (*2H*). The macroscopic solution thus obtained will be considered the "reference" or "benchmark" solution against which the results of the macroscopic model will be compared. As the microscopic solution was obtained based on a time averaged simulation (RANS equations), the macroscopic variables also need to be expressed as a function of time averaged quantities.

The definition of the MTKE introduced in the model is simply the total kinetic energy minus the filtered kinetic energy or, alternatively, it is the kinetic energy filtered in the averaging process. These two physical definitions are mathematically given by the following formula that expresses *k* as a function of mean velocities and the microscopic TKE:

$$2k = \left\langle \overline{(u_j - \langle \overline{u_j} \rangle^f)(u_j - \langle \overline{u_j} \rangle^f)} \right\rangle^f = \langle \overline{u_j u_j} \rangle^f - \langle \overline{u_j} \rangle^f \langle \overline{u_j} \rangle^f = \\ = 2k_{NK} + \langle \overline{u_j}\,\overline{u_j} \rangle^f - \langle \overline{u_j} \rangle^f \langle \overline{u_j} \rangle^f \qquad (20)$$

The numerical computing the quantity k_{NK} is straight forward as numerical simulations carried out here are based on the *k-ε* model. Explicitly, if the REV is discretized into discrete cells (or control volumes) and k_{ij} is the TKE in the cell *ij* calculated from the microscopic simulations, then *k*, using equation (20), can be expressed in terms of the variables that can be obtained from microscopic simulations, as:

$$k \cong \underbrace{\frac{1}{2H^2 f}\sum_{ij} k_{ij} C_{ij}}_{k_{NK}} + \frac{1}{2}\frac{1}{2H^2 f}\sum_{ij}(\overline{u_{ij}}\,\overline{u_{ij}} + \overline{v_{ij}}\,\overline{v_{ij}})C_{ij} - \\ -\frac{1}{2}\left(\frac{1}{2H^2 f}\right)^2\left[\left(\sum_{ij}\overline{u_{ij}}C_{ij}\right)^2 + \left(\sum_{ij}\overline{v_{ij}}C_{ij}\right)^2\right] \qquad (21)$$

where the volume of each cell is C_{ij}, $2H^2 f$ is the fluid volume of the REV, and $\overline{u_{ij}}$ and $\overline{v_{ij}}$ are the streamwise and vertical components of the mean velocity vector, respectively.

In a similar fashion, the macroscopic dissipation rate (MDR, ε) can be expressed in terms of the variables computed in the microscopic solution. Based on the definition of the MDR, it is noted that for fully developed macroscopic flow ($\langle \overline{u_i} \rangle^f$ is constant due to 1D-flow):

$$e = n\left\langle \frac{\partial^i u_i'}{\partial x_j}\frac{\partial^i u_i'}{\partial x_j}\right\rangle^f = n\left\langle \frac{\partial(\overline{{}^i u_i} + u_i')}{\partial x_j}\frac{\partial(\overline{{}^i u_i} + u_i')}{\partial x_j}\right\rangle^f = n\left\langle \frac{\partial \overline{{}^i u_i}}{\partial x_j}\frac{\partial \overline{{}^i u_i}}{\partial x_j} + \frac{\partial u_i'}{\partial x_j}\frac{\partial u_i'}{\partial x_j}\right\rangle^f =$$

$$= n\left\langle \frac{\partial \overline{{}^i u_i}}{\partial x_j}\frac{\partial \overline{{}^i u_i}}{\partial x_j}\right\rangle^f + e_{NK} = n\left\langle \frac{\partial(\overline{u_i} - \langle \overline{u_i}\rangle^f)}{\partial x_j}\frac{\partial(\overline{u_i} - \langle \overline{u_i}\rangle^f)}{\partial x_j}\right\rangle^f + e_{NK} = \quad . \qquad (22)$$

$$= n\left\langle \frac{\partial \overline{u_i}}{\partial x_j}\frac{\partial \overline{u_i}}{\partial x_j}\right\rangle^f + e_{NK}$$

The MDR in equation (22) is expressed as a function of time averaged quantities and therefore it can be computed using the RANS solution as:

$$e \cong \underbrace{n\frac{1}{2H^2 f}\sum_{ij} e_{ij} C_{ij}}_{e_{NK}} + n\frac{1}{2H^2 f}\sum_{ij}\left(\frac{\partial \overline{u_{ij}}}{\partial x}\frac{\partial \overline{u_{ij}}}{\partial x} + \frac{\partial \overline{u_{ij}}}{\partial y}\frac{\partial \overline{u_{ij}}}{\partial y} + \frac{\partial \overline{v_{ij}}}{\partial x}\frac{\partial \overline{v_{ij}}}{\partial x} + \frac{\partial \overline{v_{ij}}}{\partial y}\frac{\partial \overline{v_{ij}}}{\partial y}\right) C_{ij} \; . \qquad (23)$$

where ε_{ij} is the dissipation rate in the ij-th control volume.

4.5 Macroscopic turbulence quantities

The results of the macroscopic turbulence model are compared with the macroscopic "benchmark" results obtained in the previous section. Turbulence quantities obtained from the microscopic simulations with those yielded by the macroscopic turbulence model described. The set of equations that describe the macroscopic model in 1-D is written as (in non dimensional form):

$$\frac{1}{f}\frac{dk^*}{dx^*} = \frac{d}{dx^*}\left[\left(a\frac{k^{*2}}{e^*} + \frac{1}{\mathrm{Re}}\right)\frac{dk^*}{dx^*}\right] - e^* - U^*\frac{dP^*}{dx^*}, \qquad (24)$$

$$\frac{1}{f}\frac{de^*}{dx^*} = \frac{d}{dx^*}\left[\left(b\frac{k^{*2}}{e^*} + \frac{1}{\mathrm{Re}}\right)\frac{de^*}{dx^*}\right] - c\frac{e^{*2}}{k^*} + c\frac{e_\infty^*}{k_\infty^*}e^*, \qquad (25)$$

where ***dP*/dx**** will be calculated from the microscopic numerical results. The model parameters—*a*, *b* and *c*— need to be determined. Note that the values of the corresponding model parameters for the clear flow case are unlikely to be applicable to the porous media case.

4.6 Evaluation of model parameters

The corresponding values of the parameters in the standard k-ε model for the clear flow equations are: $a = C_m / s_k = 0.09$, $b = C_m / s_e = 0.069$ and $c = C_{e2} = 1.92$. These values are expected to be significantly different for the porous media model as the problem is described by the macroscopic quantities. For example, the microscopic level molecular diffusion, turbulent diffusion and dispersion in the transverse direction, may enhance the diffusion (coefficients *a* and *b*) in the streamwise direction at macroscopic scales. To estimate the three constants for the porous medium under study (with a uniform porosity and constant ***Re***

number), it is assumed that these coefficients are independent of the inlet BCs. Six microscopic simulations are carried out with six different boundary conditions. Following the procedure described in the previous section, reference macroscopic solutions are obtained from these microscopic results. Solutions obtained using the macroscopic model (equations 24 and 25) with different sets of parameters (*a*, *b* and *c*) are then compared with the reference solutions. The constants are estimated by minimizing the error for all six cases.

For each microscopic simulation corresponding to the inlet boundary conditions in Figure 3 (Table 1), microscopic results are integrated in the first (inlet) REV of the porous medium to yield an inlet macroscopic boundary condition for the macroscopic model. Additionally, the fully developed macroscopic values are computed from microscopic results to be used as the boundary condition at the exit for the macroscopic model. Table 2 shows values thus computed for different microscopic inlet BCs.

Microscopic inlet BCs	Macroscopic BCs (75% porosity)					
	Inlet		Inlet/Outlet		Outlet	
	k^*	ε^*	k^* / k_∞^*	$\varepsilon^* / \varepsilon_\infty^*$	k_∞^*	ε_∞^*
Set 1	1.20	1.61	0.77	0.42	1.55	3.80
Set 2	1.09	1.74	0.70	0.46		
Set 3	1.08	1.89	0.69	0.50		
Set 4	1.11	2.13	0.72	0.56		
Set 5	1.23	2.53	0.79	0.66		
Set 6	1.37	2.95	0.88	0.78		

Table 2. Macroscopic turbulence quantities at the inlet and outlet computed for each set of microscopic BCs.

Values tabulated in Table 2 are used as boundary values to numerically solve the macroscopic model equations (24 and 25). These solutions are obtained in a macroscopic domain that extends from $x / H = 0$ to $x / H = 14$, using a non regular grid with a total of 1000 grid points (geometric grid, finer grid at the inlet, geometric ratio = 1.0015). Diffusion terms are approximated with central differences and the convective term with the first order upwind scheme. The system of equations for the macroscopic turbulence quantities is solved using a LU decomposition as a boundary value problem for each turbulence variable in a segregated scheme. The solution is under-relaxed, the eddy viscosity is recalculated, and the linear systems are solved iteratively until convergence is achieved. Results are tested to be independent of the location of the outlet boundary condition and grid size.

The volume average results of the microscopic solution are interpolated (linearly) on to the macroscopic grid and compared to the macroscopic solution obtained for each set of model parameters. A relative quadratic error is defined for each inlet BC and each set of parameters as:

$$error_j(a,b,c) = \frac{1}{N}\sum_i^N (k_{macro}(i)/k_{micro}(i) - 1)^2 + (e_{macro}(i)/e_{micro}(i) - 1)^2 , \qquad (26)$$

where *j* refers to each case in the set of (six) inlet BCs, *i* indicates each of the *N* grid points of the discretization and macro and micro refers to macroscopic solution (for each *a*, *b* and *c*) and space averaged microscopic solution, respectively. Preliminary evaluation of the error showed that the coefficient *c* is relatively close to its original value for the clear flow case ($c \approx 1.92$) independent of the BC, and the diffusion coefficients have a relatively large impact on the

solution. Based on this preliminary insight, two simulations are carried out for each *j*-error. In the first one, both *a* and *b*, are varied from 0.05 to 10 with a step of 0.05 and *c* is fixed at 1.9. This simulation provides a minimum total error (i.e. sum over all BCs or *j* in equation 26) with values of *a* and *b* lower than 1. Therefore, in the second simulation, *a* and *b* are varied from 0.025 to 1 with a step of 0.025 and c is varied from 1 to 3 with a step of 0.1.

The objective of this error-minimization study is not to evaluate the values of the coefficients under consideration precisely but, as an intermediate step, to evaluate if the model has the capability to fairly predict the space averaged microscopic behavior with a fixed set of model parameters. For instance, for the problem under study, the diffusion in the streamwise direction may be expected to be of a lower order than source and convective terms. Therefore, this problem may not be the best choice to compute the diffusion coefficients. Additionally, the reader may note that the definition of the error given in equation (26) is somewhat arbitrary, and so is the definition of the overall error ($\sum error_j$). A different choice of these definitions may lead to a slightly different set of optimal values for the model parameters.

4.7 Results

Top six rows of Table 3 show the summary of the results obtained using the values of *a*, *b* and *c* (the model parameters) that minimize the error for each BC. The spread of the calculated model parameters is acceptable. Coefficients *a* and *c* are largely independent of the BCs (a = 0.025 and c = 1.9). Coefficient b needs to be varied between 0.025 and 1.3 to minimize the error for the six different BCs. The overall error ($\sum error_j$) for b = 0.85 is shown in the bottom row of Table 3. The overall error for this set of model parameters for all six sets of BCs is quite small (.0053) and within acceptable limits. Moreover, the error for each set of BCs ($error_j$ in Table 3) for this set of model parameters (bottom row in Table 3) is not increased by more than 20% compared to the minimum error for that set of BC (second last column in Table 3). This ratio is shown in the last column of Table 3 for each BC. This implies that the solution for all six different inlet BCs is not significantly degraded with a single optimal set of model parameters or, in other words, the solution is not strongly sensitive to the value of this parameter (b) over the range of BCs under consideration.

Boundary conditions	a	b	c	$error_j$*1000	$error_j$ /$error_{jT}$ (%)
Set 1	0.025	1.3	1.9	1.5	4.3
Set 2	0.025	1.0	1.9	1.0	0.8
Set 3	0.025	0.7	1.9	0.8	0.6
Set 4	0.025	0.25	1.9	0.6	8.3
Set 5	0.025	0.25	1.9	0.5	18.3
Set 6	0.025	0.025	1.9	0.5	19.7
Overall	0.025	0.875	1.9	5.3	-

Table 3. Parameter values for the macroscopic model and errors between microscopic and macroscopic results for each BC.

Macroscopic solutions obtained using the optimal set of parameters given by a = 0.025, b = 0.875 and c = 1.9, are compared with the microscopic ones in Figures 5-7 for the six inlet BCs (error bars correspond to a ±10% error with respect to the averaged microscopic solution). The agreement between the reference solution and the macroscopic results is fairly good validating the capabilities of the model to predict macroscopic turbulence quantities. Largest

discrepancies are found for BC Set 1, but the errors even for this worst case are within a 10% error bar.

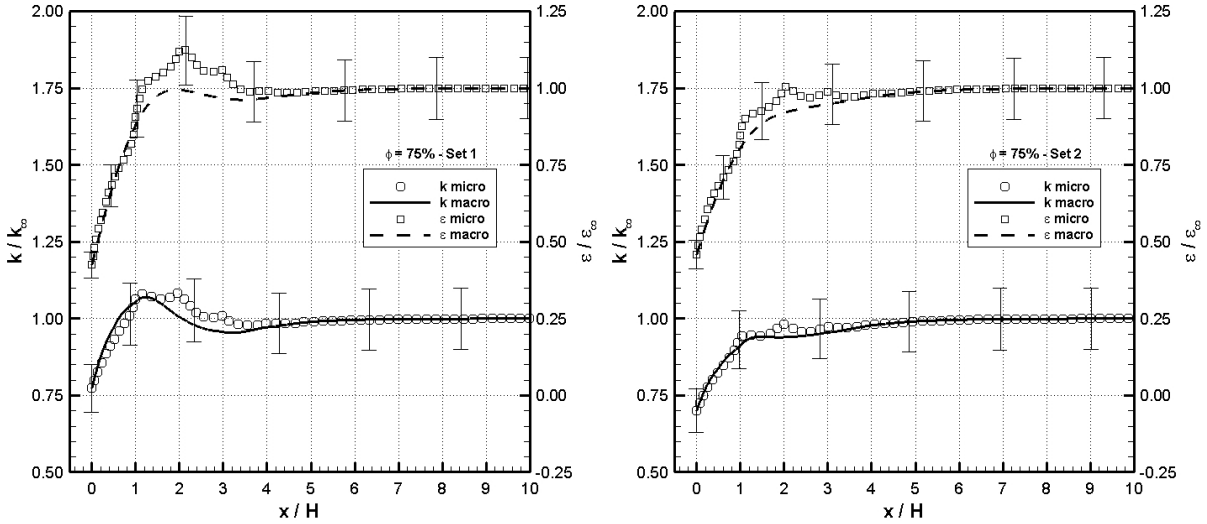

Figure 5. Streamwise evolution of the MTKE and the MDR calculated using the microscopic and the macroscopic models. BC Set 1 (left panel) and BC Set 2 (right panel).

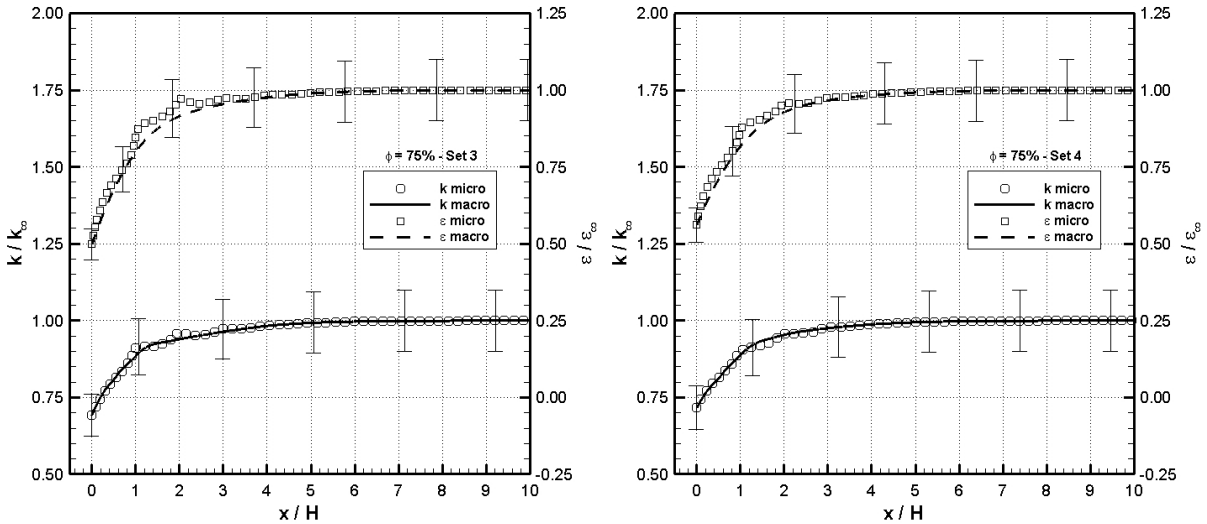

Figure 6. Streamwise evolution of the MTKE and the MDR calculated using the microscopic and the macroscopic models. BC Set 3 (left panel) and BC Set 4 (right panel).

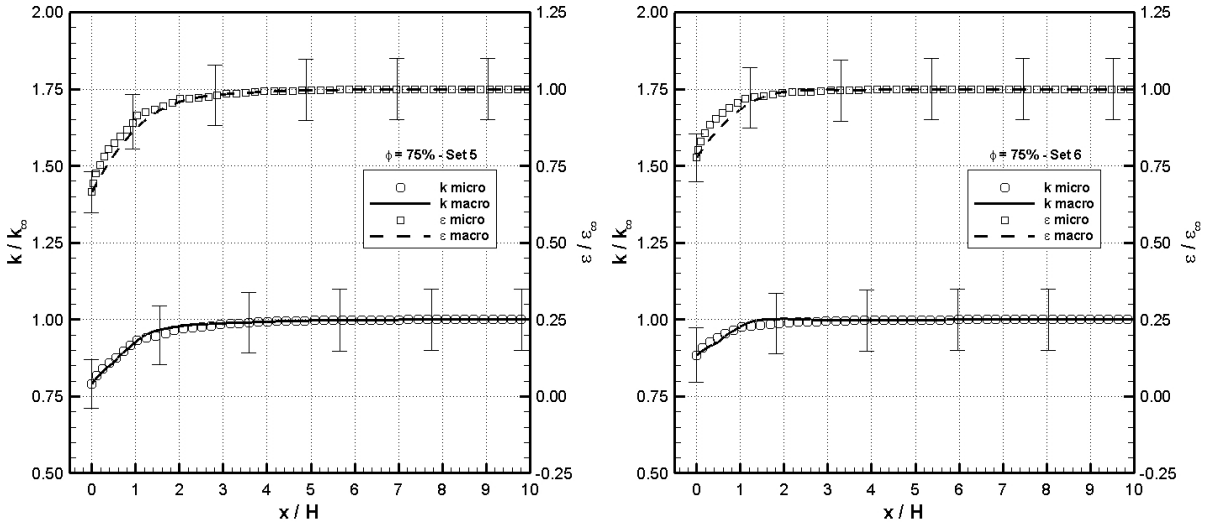

Figure 7. Streamwise evolution of the MTKE and the MDR calculated using the microscopic and the macroscopic models. BC Set 5 (left panel) and BC Set 6 (right panel).

5 CONCLUSION

The set of macroscopic equations presented and validated in this study is shown to have several positive features. For developing flow, a set of optimal model parameter values are determined by comparing the results of the macroscopic model with reference data for a set of six different inlet boundary conditions. The comparison of numerical results obtained using the model developed here with averaged microscopic results showed satisfactory agreement. The 75% porosity case was tested using the optimal set of model parameters and showed excellent agreement with reference microscopic results for both turbulence quantities for the entire range of inlet turbulent intensities.

The simple flow (from the macroscopic point of view) studied here proved to be very useful to carry out the first steps in the evaluation of the turbulence model in porous media. Overall, it is concluded that the model captures the flow characteristics very well over a large range of boundary conditions.

REFERENCES

Abe, K., Kondoh, T. and Nagano, Y., A new turbulence model for predicting fluid flow and heat transfer in separating and reattaching flows-l. Flow field calculations. *International Journal of Heat and Mass Transfer* 37:139-151, 1994.

Antohe, B.V. and Lage, J.L., A general two-equation macroscopic turbulence model for incompressible flow in porous media. *International Journal of Heat and Mass Transfer*, 40:3013-3024, 1997.

Becker, S. and Laurien, E., Three-dimensional numerical simulation of flow and heat transport in high-temperature nuclear reactors. *Nuclear Engineering and Design*, 222:189-201, 2003.

Chandesris, M., Serre, G. and Sagaut, P., A macroscopic turbulence model for flow in porous media suited for channel, pipe and rod bundle flows. *International Journal of Heat Mass Transfer*, 49:2735-2750, 2006.

Gray, W.G., Leijnse, A., Kolar, R.L. and Blain, C.A., Mathematical Tools for Changing Spatial Scales in the Analysis of Physical Systems, CRC Press, 1993.

Hassanizadeh, M. and Gray, W.G., General conservation equations for multi-phase systems: 1. Averaging procedure. *Advance in Water Resources*, 2:131-144, 1979.

Hayase, T., Humphrey, J.A.C., and Greif, R., A Consistently formulated QUICK scheme for fast and stable convergence using finite-volume iterative calculation procedures. *Journal of Computational Physics* 98:108-l 18, 1982.

Kaviany, M., Principles of Heat Transfer in Porous Media, Springer-Verlag, 1991.

Leonard, B.P., A stable and accurate convective modeling procedure based on quadratic upstream interpolation. *Computer Methods in Applied Mechanics Engineering*, 19:59-98, 1979.

Lopez, F. and Garcia, M.H., Mean flow and turbulence structure of open-channel flow through non-Emergent vegetation. *Journal of Hydraulic Engineering*, 127:392-402, 2001.

Masuoka, T. and Takatsu, Y., Turbulence model for flow through porous media. *International Journal of Heat Mass Transfer*, 39:2803-2809, 1996.

Nakayama, A. and Kuwahara, F., A macroscopic turbulence model for flow in a porous medium. *Journal of Fluids Engineering*, 121:427-433, 1999.

Nakayama, A., Kuwahara, F. and Hayashi, T., Numerical modelling for three-dimensional heat and fluid flow through a bank of cylinders in yaw. *Journal of Fluid Mechanics*, 428:139–159, 2004.

Patankar, S.V., Numerical Heat Transfer and Fluid Flow, Hemisphere, 1980.

Pedras, M.H.J. and de Lemos, M.J.S., On the definition of turbulent kinetic energy for flow in porous media. *International Communications on Heat and Mass Transfer* 27:211-220, 2000.

Pedras, M.H.J. and de Lemos, M.J.S., Macroscopic turbulence modeling for incompressible flow through undeformable porous media. *International Journal of Heat Mass Transfer*, 44:1081-1093, 2001.

Quintard, M. and Whitaker, S., Transport in ordered and disordered porous media II: generalized volume averaging. *Transport in Porous Media* 14:179-206, 1994.

Raupach, M.R. and Shaw, R.H., Averaging procedures for flow within vegetation canopies. *Boundary-Layer Meteorology* 22:79-90, 1982.

Teruel, F.E. and Rizwann-uddin, Alternative modeling for turbulent flow in porous media. In Proceedings of the 2nd joint U.S.-European Fluid Engineering Summer Meeting, 2006.

Teruel, F.E., Macroscopic turbulence modeling and simulation for flow through porous media. PhD thesis, University of Illinois, Urbana-Champaign, IL, 2007.

Whitaker, S., Advances in theory of fluid motion in porous media. *Industrial and Engineering Chemistry*, 61:14-28, 1969.

Whitaker, S., The Method of Volume Averaging, Kluwer, 1999.